and spectroscopy applications [for a review, see Riekel (2000)]. The choice of materials has evolved, too, from the relatively easy-to-work-with and -finish fused quartz to silicon; silicon having the advantageous property that at liquid-nitrogen temperature the expansion coefficient is zero (Bilderback, 1986). This has been of particular advantage in the cooling of silicon monochromators at the ESRF, where the heat loading on optics is very high. An alternative approach with the rather small X-ray beams from undulators is the use of transparent monochromator crystals made of diamond, which is a robust material with the additional advantage of transparency, thus allowing multiplexing of stations, one downstream from the other, fed by one straight section of one or more undulator designs. For a review of the ESRF beamline optics, see Freund (1996); for reviews of the macromolecular crystallography programmes at the ESRF, see Miller (1994), Branden (1994) and Lindley (1999), as well as the *ESRF Foundation Phase Report* (1987). See also Helliwell (1992), Chapter 5.

Detectors have improved enormously. The early days of SR use saw considerable reliance on photographic film, as well as single-counter four-circle diffractometers. Evolution of area detectors, in particular, has been considerable and impressive, and in a variety of technologies. Gas detectors, *i.e.*, the multiwire proportional chamber (MWPC), were invented and developed through various generations and types [Charpak (1970); for reviews of their use at SR sources, see *e.g.* Lewis (1994) and Fourme (1997)]. MWPCs have the best detector quantum efficiency (DQE) of the area detectors, but there are limitations on count rate (local and global) and their use at wavelengths less than ~1 Å is restricted due to geometric image parallax effects. The most popular devices at present are charge coupled devices (CCDs) [see Tate *et al.* (1995), Allinson (1994), Gruner & Ealick (1995) and Westbrook & Naday (1997) for details of their development]. Image plates (IPs) were popular during the late 1980s and early to mid-1990s, mainly, but not exclusively, with online scanners, notably the MAR Research devices. IPs are also used in a Weissenberg geometry [see Sakabe (1983, 1991) and Sakabe *et al.* (1995), and for a recent review see Amemiya (1997)]. IPs and CCDs are complementary in performance, especially with respect to size and duty cycle; IPs are larger, *i.e.*, with many resolution elements possible, but are slower to read out than CCDs. Both are capable of imaging well at wavelengths shorter than 1 Å and with high count rates. Both have overcome the tedium of chemical development of film. Other detectors needed for crystallography include those for monitoring the beam intensity; these must not interfere with the beam collimation, and yet must monitor the beam downstream of the collimator (Bartunik *et al.*, 1981); also needed are fluorescence detectors for setting the wavelength for optimized anomalous-scattering applications (see Cianci *et al.*, 2005).

Most recently, an area-detector development has been the so-called pixel detector. This is made of silicon cells, each 'bump bonded' onto associated individual electronic readout chains. Thus, extremely high count rates are possible. These devices can then combine the attributes of large image plate sensitive areas with the fast readout of CCDs, along with high count-rate capability and so on. Devices and prototypes have been developed at Princeton/Cornell (Eikenberry *et al.*, 1998), Berkeley/San Diego (Beuville *et al.* 1997) and Imperial College, London (Hall, 1995), and are now in use at the SLS (Broennimann *et al.*, 2006).

Provision of robotics for sample mounting on the synchrotron beamlines has been increasingly deployed in the last decade, improving efficiency and ease of use, often coupled with remote access (*e.g.* see Gonzalez *et al.*, 2005) and telepresence (*e.g.* see Warren *et al.*, 2008).

8.1.7. SR monochromatic and Laue diffraction geometry

In the utilization of SR, both Laue and monochromatic modes are important for data collection. The unique geometric and spectral properties of SR render the treatment of diffraction geometry different from that for a conventional X-ray source.

8.1.7.1. Laue geometry: sources, optics, sample reflection bandwidth and spot size

Laue geometry involves the use of the polychromatic SR spectrum as transmitted through the beryllium window that is used to separate the apparatus from the machine vacuum. There is useful intensity down to a wavelength minimum of $\sim\lambda_c/5$, where λ_c is the critical wavelength of the magnet source in the case of bending magnets (BMs) and wavelength shifters. The maximum wavelength is typically $\geq$3 Å; however, if the crystal is mounted in a capillary, then the glass absorbs the wavelengths beyond ~2.5 Å (Helliwell, 2004).

The bandwidth on BMs and wigglers can be limited by a reflecting mirror at grazing incidence, whereby the minimum wavelength in the beam can be sharply defined to aid the accurate definition of the Laue spot multiplicity. The mirror can also be used to focus the beam at the sample. The maximum-wavelength limit can be truncated by use of aluminium absorbers of varying thickness or a transmission mirror (Lairson & Bilderback, 1982; Cassetta *et al.*, 1993).

The measured intensity of individual Laue diffraction spots depends on the wavelength at which they are stimulated. The problem of wavelength normalization is treated by a variety of methods. These include:

(i) use of a monochromatic reference data set;
(ii) use of symmetry equivalents and multiple measurements in the Laue data set recorded at different wavelengths;
(iii) calibration with a standard sample, such as a silicon crystal.

Each of these methods produces a 'λ curve' describing the relative strength of spots measured at various wavelengths. Most Laue diffraction data are now recorded on CCDs or IPs. The greater sensitivity of these detectors (expressed as the DQE), especially for weak signals, has greatly increased the number of Laue exposures recordable per crystal (*e.g.* Nieh *et al.*, 1999). Thus, multiplet deconvolution procedures, based on the recording of reflections stimulated at different wavelengths and with different relative intensities, have become possible (Campbell & Hao, 1993; Ren & Moffat, 1995*b*; Nieh *et al.*, 1999). Data quality and completeness have improved considerably.

Narrow-bandpass beams, *e.g.* $\delta\lambda/\lambda \leq 0.2$, are used for enhancing the signal-to-noise ratio. Such bandwidths are produced generally by an X-ray undulator, whereby *e.g.* 10–100 periods should ideally yield a bandwidth behind a pinhole of $\delta\lambda/\lambda \simeq 0.1$–0.01. In these cases, wavelength normalization is more difficult, because the actual spectrum over which a reflection is integrated is rapidly varying in intensity; nevertheless, high-order Chebychev polynomials are successful (Ren & Moffat, 1995*a*; Artz *et al.*, 1999).

The spot bandwidth is determined by the mosaic spread and horizontal beam divergence (since $\gamma_H > \gamma_V$) as

$$(\delta\lambda/\lambda) = (\eta + \gamma_H)\cot\theta, \qquad (8.1.7.1)$$

where η is the sample mosaic spread, assumed to be isotropic, and

γ_H is the horizontal cross-fire angle, which in the absence of focusing is $(x_H + \sigma_H)/P$, where x_H is the horizontal sample size, σ_H is the horizontal source size and P is the sample to the tangent-point distance. This is similar for γ_V in the vertical direction. Generally, at SR sources, σ_H is greater than σ_V. When a focusing-mirror element is used, γ_H and/or γ_V are convergence angles determined by the focusing distances and the mirror aperture.

The size and shape of the diffraction spots vary across the detector image plane. The radial spot length is given by convolution of Gaussians as

$$\left(L_R^2 + L_c^2 \sec^2 2\theta + L_{\rm PSF}^2\right)^{1/2} \qquad (8.1.7.2)$$

and tangentially by

$$\left(L_T^2 + L_c^2 + L_{\rm PSF}^2\right)^{1/2}, \qquad (8.1.7.3)$$

where L_c is the size of the X-ray beam (assumed to be circular) at the sample, $L_{\rm PSF}$ is the detector point-spread factor,

$$L_R = D \sin(2\eta + \gamma_R) \sec^2 2\theta, \qquad (8.1.7.4)$$

$$L_T = D(2\eta + \gamma_T) \sin\theta \sec 2\theta, \qquad (8.1.7.5)$$

and

$$\gamma_R = \gamma_V \cos\psi + \gamma_H \sin\psi, \qquad (8.1.7.6)$$

$$\gamma_T = \gamma_V \sin\psi + \gamma_H \cos\psi, \qquad (8.1.7.7)$$

where ψ is the angle between the vertical direction and the radius vector to the spot (see Andrews *et al.*, 1987). For a crystal that is not too mosaic, the spot size is dominated by L_c and $L_{\rm PSF}$. For a mosaic or radiation-damaged crystal, the main effect is a radial streaking arising from η, the sample mosaic spread.

8.1.7.2. Monochromatic SR beams: optical configurations and sample rocking width

A wide variety of perfect-crystal monochromator configurations are possible and have been reviewed by various authors (Hart, 1971; Bonse *et al.*, 1976; Hastings, 1977; Kohra *et al.*, 1978). Since the reflectivity of perfect silicon and germanium is effectively 100%, multiple-reflection monochromators are feasible and permit the tailoring of the shape of the monochromator resolution function, harmonic rejection and manipulation of the polarization state of the beam. Two basic designs are in common use. These are the bent single-crystal monochromator of triangular shape (Fig. 8.1.4.1*a*) and the double-crystal monochromator (Fig. 8.1.4.1*b*).

8.1.7.2.1. Curved single-crystal monochromator

In the case of the single-crystal monochromator, the actual curvature employed is very important in the diffraction geometry. For a point source and a flat monochromator crystal, there is a gradual change in the photon wavelength selected from the white beam as the length of the monochromator is traversed (Fig. 8.1.7.1*a*). For a point source and a curved monochromator crystal, one specific curvature can compensate for this variation in incidence angle (Fig. 8.1.7.1*b*). The reflected spectral bandwidth is then at a minimum; this setting is known as the 'Guinier position'. If the curvature of the monochromator crystal is increased further, a range of photon wavelengths, $(\delta\lambda/\lambda)_{\rm corr}$, is selected along its length so that the rays converging towards the focus have a correlation of photon wavelength and direction (Fig. 8.1.7.1*c*). The effect of a finite source is to cause a change in incidence angle at the monochromator crystal, so that at the focus there is a photon-wavelength gradient across the width of the focus (for all curvatures) (Fig. 8.1.7.1*d*). The use of a slit in the focal plane is akin to placing a slit at the tangent point to limit the source size.

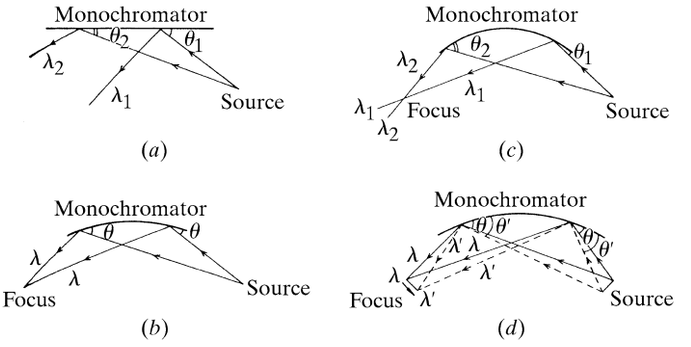

Figure 8.1.7.1
Single-crystal monochromator illuminated by SR. (*a*) Flat crystal. (*b*) Guinier setting. (*c*) Overbent crystal. (*d*) Effect of source size (shown at the Guinier setting for clarity). From Helliwell (1984). Reproduced with the permission of the Institute of Physics.

8.1.7.2.2. Double-crystal monochromator

The double-crystal monochromator with two parallel or nearly parallel perfect crystals of germanium or silicon is a common configuration. The advantage of this is that the outgoing monochromatic beam is parallel to the incoming beam, although it is slightly displaced vertically by an amount $2d\cos\theta$, where d is the perpendicular distance between the crystals and θ is the monochromator Bragg angle (unless the second crystal is unconnected to the first, in which case it can be translated as well to compensate for that). The monochromator can be rapidly tuned, since the diffractometer or camera need not be re-aligned significantly in a scan across an absorption edge. Since the rocking width of the fundamental is broader than the harmonic reflections, the strict parallelism of the pair of the crystal planes can be 'detuned', so that the harmonic can be rejected with little loss of the fundamental intensity. The spectral spread in the reflected monochromatic beam is determined by the source divergence accepted by the monochromator, the angular size of the source and the monochromator rocking width (see Fig. 8.1.7.2). The double-crystal monochromator is often used with a toroidal focusing mirror; the functions of monochromatization are then separated from the focusing (Hastings *et al.*, 1978).

8.1.7.2.3. Widening of monochromatic wavelength range provision

Users and facilities have been driven to use an ever-widening practical range of X-ray wavelengths. Longer wavelengths in protein crystallography have been explored up to 2.6 Å (Helliwell, 1993, 1997*a*, 2004; Polikarpov *et al.*, 1997; Teplyakov *et al.*, 1998; Cianci *et al.*, 2001, 2008), and even softer wavelengths have been under active development to utilize the uranium *M* edge at 3.326 and 3.490 Å (Liu *et al.*, 2001), and the S *K* edge for anomalous dispersion (Stuhrmann & Lehmann, 1994). At very short (~0.5 Å) and ultra-short (~0.3 Å) wavelengths, a high machine energy yields copious flux output; pilot studies have been conducted in protein crystallography at CHESS (Helliwell *et al.*, 1993), at the ESRF (Schiltz *et al.*, 1997) and at the NSLS (Jakoncic *et al.*, 2006). Notably Fourme and colleagues have exploited the condensed angular distribution of the diffraction pattern at such wavelengths to pass the beam through the narrow

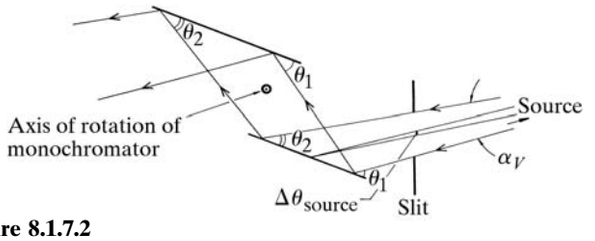

Figure 8.1.7.2
Double-crystal monochromator illuminated by SR. The contributions of the source divergence, α_V [less than or equal to γ^{-1}, equation (8.1.2.4), depending on the monochromator vertical entrance slit aperture; see also Colapietro *et al.* (1992)], and angular source size, $\Delta\theta_{\text{source}}$, to the range of energies reflected by the monochromator are shown. From Helliwell (1984). Reproduced with the permission of the Institute of Physics.

exit window of a high-pressure cell for protein-crystal high-pressure biophysical studies (Fourme *et al.*, 2001; Girard *et al.*, 2007). Such developments interact closely with machine and beamline specifications.

8.1.7.2.4. Crystal sample rocking width

The rocking width of a reflection depends on the horizontal and vertical beam divergence or convergence (after due account for collimation is taken), γ_H and γ_V, the spectral spreads $(\delta\lambda/\lambda)_{\text{conv}}$ and $(\delta\lambda/\lambda)_{\text{corr}}$, and the mosaic spread, η. We assume that the mosaic spread η is $\gg \omega$, the angular broadening of a reciprocal-lattice point (relp) due to a finite sample. In the case of synchrotron radiation, γ_H and γ_V are usually widely asymmetric. On a conventional source, usually $\gamma_H \simeq \gamma_V$. Two types of spectral spread occur with synchrotron (and neutron) sources. The term $(\delta\lambda/\lambda)_{\text{conv}}$ is the spread that is passed down each incident ray in a divergent or convergent incident beam; the subscript refers to the conventional source type. This is because it is similar to the $K\alpha_1, K\alpha_2$ line widths and separation. At the synchrotron, this component also exists and arises from the monochromator rocking width and finite-source-size effects. The term $(\delta\lambda/\lambda)_{\text{corr}}$ is special to the synchrotron or neutron case. The subscript 'corr' refers to the fact that the ray direction can be correlated with the photon or neutron wavelength. In this most general case, and for one example of a $(\delta\lambda/\lambda)_{\text{corr}}$ arising from the horizontal ray direction correlation with photon energy and the case of a horizontal rotation axis, the rocking width φ_R of an individual reflection is given by

$$\varphi_R = \left\{L^2\left[(\delta\lambda/\lambda)_{\text{corr}} d^{*2} + \zeta\gamma_H\right]^2 + \gamma_V^2\right\}^{1/2} + 2\varepsilon_s L, \qquad (8.1.7.8)$$

where

$$\varepsilon_s = (d^* \cos\theta/2)\left[\eta + (\delta\lambda/\lambda)_{\text{conv}} \tan\theta\right] \qquad (8.1.7.9)$$

and L is the Lorentz factor, $1/\left(\sin^2 2\theta - \zeta^2\right)^{1/2}$.

The Guinier setting of an instrument (curved crystal monochromator case, Fig. 8.1.7.1*b*) gives $(\delta\lambda/\lambda)_{\text{corr}} = 0$. The equation for φ_R then reduces to

$$\varphi_R = L\left[\left(\zeta^2\gamma_H^2 + \gamma_V^2/L^2\right)^{1/2} 2\varepsilon_s\right] \qquad (8.1.7.10)$$

(from Greenhough & Helliwell, 1982). For example, for $\zeta = 0$, $\gamma_V = 0.2$ mrad (0.01°), $\theta = 15°$, $(\delta\lambda/\lambda)_{\text{conv}} = 1 \times 10^{-3}$ and $\eta = 0.8$ mrad (0.05°), then $\varphi_R = 0.08°$. But φ_R increases as ζ increases [see Greenhough & Helliwell (1982), Table 5]. In the rotation/oscillation method as applied to protein and virus crystals, a small angular range is used per exposure. For example, the maximum rotation range per image, $\Delta\varphi_{\text{max}}$, may be 1.5° for a protein and

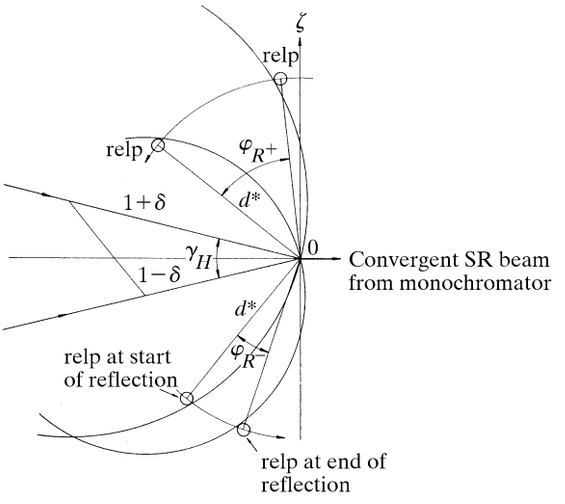

Figure 8.1.7.3
The rocking width of an individual reflection for the case of Fig. 8.1.7.1(*c*) and a vertical rotation axis. From Greenhough & Helliwell (1982).

0.4° or so for a virus. Many reflections will be only partially stimulated over the exposure. It is important, especially in the virus case, to predict the degree of penetration of the relp through the Ewald sphere. This is done by analysing the interaction of a spherical volume for a given relp with the Ewald sphere. The radius of this volume is given by

$$E \simeq \varphi_R/2L \qquad (8.1.7.11)$$

(Greenhough & Helliwell, 1982).

In Fig. 8.1.7.3, the relevant parameters are shown. The diagram shows $(\delta\lambda/\lambda)_{\text{corr}} = 2\delta$ in a plane, usually horizontal with a perpendicular (vertical) rotation axis, whereas the formula for φ_R above is for a horizontal axis. This is purely for didactic reasons since the interrelationship of the components is then much clearer.

The limits of protein-crystal rocking widths have been explored by Helliwell (1988), Colapietro *et al.* (1992) and Snell (1995), whereby arc-second crystal precision has been observed at room temperature, *i.e.* unfrozen protein crystals. Special analysis software (Lovelace *et al.*, 2000) has been written to extract such precise crystal mosaicity values and the experiment obviously requires stringent (usually undulator) collimation. Exact comparisons of mosaicity values need reflection indexing, *e.g.* see Snell *et al.* (1995).

8.1.8. Scientific utilization of SR in protein crystallography

There are a myriad of applications and results of the use of SR in crystallography. Helliwell (1992) gave an extensive survey and tabulations of SR and macromolecular crystallography applications; Chapter 9 therein concentrates on anomalous scattering and Chapter 10 on high resolution, large unit cells, small crystals, weak scattering efficiency and time-resolved data collection. The field has expanded so dramatically, in fact, that an equivalent survey today would be vast. Table 8.1.4.1 lists the web pages of the facilities, where the specifications and details of the beamlines can be found (*e.g.* all the publications at Daresbury in the protein crystallography area organized by beamline instrument are to be found at http://dlwebres.dl.ac.uk/dl_public/publications/index.jsp). The examples below cite extreme cases of the large unit cell (virus and multi-macromolecular) cases, weak anomalous-scattering signal in MAD, fast time-resolved Laue